Rotating black hole mimicker surrounded by the string cloud

Yi Yang,[1,*] Dong Liu,[2,†] Ali Övgün,[3,‡] Gaetano Lambiase,[4,5,§] and Zheng-Wen Long[2,‖]

[1]*School of Mathematics and Statistics, Guizhou University of Finance and Economics, Guiyang 550025, China*

[2]*College of Physics, Guizhou University, Guiyang 550025, China*

[3]*Physics Department, Eastern Mediterranean University, Famagusta, 99628 North Cyprus via Mersin 10, Turkey*

[4]*Dipartimento di Fisica "E.R Caianiello", Università degli Studi di Salerno, Via Giovanni Paolo II, 132–84084 Fisciano (SA), Italy*

[5]*Istituto Nazionale di Fisica Nucleare—Gruppo Collegato di Salerno—Sezione di Napoli, Via Giovanni Paolo II, 132–84084 Fisciano (SA), Italy*

(Received 30 October 2023; accepted 12 December 2023; published 2 January 2024)

Traversable wormholes and regular black holes usually represent completely different scenarios. But in the black bounce spacetime they can be described by a same line element, which is very attractive. Furthermore, the black hole photos taken by EHT show that black holes have spin, so spin is an indispensable intrinsic property of black holes in the actual Universe. In this work, we derive a rotating black hole mimicker surrounded by the string cloud (SC), which can be interpolated to represent regular black hole spacetime and traversable wormhole spacetime. We investigate the effect of the spin a and SC parameter L on the observables (shadow radius R_s and distortion δ_s) and energy emission rate of the black hole mimicker surrounded by the SC. We find that shadow for this spacetime is very sensitive to the L, i.e., the SC parameter can significantly increase the boundary of the shadow.

DOI: 10.1103/PhysRevD.109.024002

I. INTRODUCTION

Einstein proposed the extremely important general relativity (GR) in 1915. General relativity explains gravity as the curvature of spacetime. Black holes are a very important prediction of GR. In 1916, Schwarzschild [1] solved the Einstein field equations to obtain a static spherical symmetric vacuum solution, which described a nonrotating black hole with only mass. In 1963, Kerr obtained a rotating, steady-state axisymmetric vacuum black hole solution [2]. In the classical gravity theory, there is a singularity inside the black hole [3]. Singularities represent points where geodesics terminate abruptly, therefore their appearance often heralds the collapse of the gravity theory. It is generally believed that singularities must be eliminated by quantum gravity theory effects, but so far there is no satisfactory quantum gravity theory. Therefore, studies on the properties of classical regular black holes have attracted much attention in recent years [4–8]. Bardeen first obtained a kind of regular black hole without singularity, which was later called the Bardeen black hole [9]. Simpson and Visser proposed a black-bounce spacetime, which can use the same line element to describe regular black holes, one-way traversable wormholes, and two-way traversable wormholes [10]. In Refs. [11,12], Pal *et al.* used the Simpson-Visser method to regularize a few naked singularity spacetimes, where they interpreted the geometry as an exact solution of nonlinear electrodynamics. Mazza *et al.* [13] extended the Simpson-Visser metric (SVM) to the rotating case by using the Newman-Janis (NJ) algorithm, where the NJ algorithm is a very suitable method for extending Schwarzschild-like black holes to Kerr-like black holes [14–16]. Furthermore, in Ref. [17] the authors constructed the rotating version of the Simpson-Visser geometry, which can be used as an alternative to the Kerr black hole.

In the realm of string theory, the fundamental constituents of the natural world are one-dimensional entities rather than zero-dimensional particles. When studying gravitational interactions, we can liken a collection of these strings to a one-dimensional counterpart of a dust cloud. It is worth noting that the idea of string clouds (SCs) was developed by Letelier in Refs. [18,19]. Taking into account the fact that, according to the string theory, the building blocks of nature are extended (one-dimensional) strings, rather than pointlike structures with zero dimension, as assumed in quantum field theory, Letelier inferred a generalized

*yiyang@mail.gufe.edu.cn
†dongliuvv@yeah.net
‡ali.ovgun@emu.edu.tr
§lambiase@sa.infn.it
‖zwlong@gzu.edu.cn

Schwarzschild solution of Einstein's equations. More precisely, this solution describes a spherically symmetric cloud (dust) of strings surrounding the standard Schwarzschild black hole. The SC alters the horizon of the black hole, compared with the Schwarzschild black hole. The entirety of this string cloud constitutes a self-contained system, ensuring the conservation of the stress-energy tensor. In Ref. [20], the authors studied the superradiance of noncommutating rotating SV spacetime. Recently, Rodrigues *et al.* [21] introduced a black hole mimicker surrounded by the string cloud, which proves that the existence of the SC makes the black-bounce spacetime remain regular. The idea of SC has been investigated in several contexts, such as missing matter (dark matter problem) [22], BHs in pure Lovelock gravity [23], Hawking radiation [24], anti–de Sitter black holes [25], $f(R)$ gravity [26] (see, also, for example Refs. [27–35] and references therein for further studies).

LIGO/Virgo first detected gravitational waves from the collision of two black holes in 2015 [36–39], which confirmed the existence of black holes predicted by general relativity. This opened a new era in gravitational wave astronomy. In 2019, the Event Horizon Telescope (EHT) released the first image of a black hole, which is the shadow of the supermassive black hole M87 at the center of the Virgo elliptical galaxy [40]. In addition, EHT released a photo of Sagittarius A* in 2022 [41], which is the supermassive black hole at the center of the Milky Way. The information carried by black hole photos can help one further understand the shadow, jet and accretion process of the black hole. In the literature, there exist numerous studies focusing on the intriguing phenomenon of black hole shadows [42–60]. In the currently released photos of black holes, the main part is the outer circular bright area and the inner dark area. The outer bright region represents the accretion disk, and the brightness of this part is not uniform. The reason for this phenomenon is that the brightness of the accretion disk is affected by the Doppler effect. The accretion disk moving toward the detector will be brighter, while moving away from the detector will be relatively darker, where the position of the bright region in the black hole shadow is closely related to the spin of a black hole. Therefore, it is necessary to introduce spin into black-bounce spacetime surrounded by the SC.

Motivated by EHT releases of the black hole image, our aim in this paper is to study the shadows of the rotating black hole mimicker surrounded by the SC, and analyze their characteristics. Such a study will provide some direction for the experimental detection of such a spacetime.

This work is organized as follows. In Sec. II, we briefly review Simpson-Visser spacetime surrounded by the SC. In Sec. III, the rotating black hole mimicker surrounded by the SC are derived by using the Newman-Janis (NJ) method. In Sec. IV, we obtain the geodesic equation by solving the Hamilton-Jacobi equation in the rotating black hole mimicker surrounded by the SC. In Sec. V, we present the shadow images of rotating black hole mimicker surrounded by the SC, and analyze the influence of spin and SC parameters on the shadow. In Sec. VI, we study the shadow radius, distortion, and energy emission rate of the rotating black hole mimicker surrounded by the SC. Section VII is our main conclusion of this work.

II. REVIEW OF THE NONROTATING BLACK HOLE MIMICKER SURROUNDED BY THE STRING CLOUD

Rodrigues *et al.* [21] derive the black bounces in a cloud of string by considering the following Einstein equations (see the Appendix for details and definitions):

$$R_{\mu\nu}-\frac{1}{2}Rg_{\mu\nu}=\kappa^2T_{\mu\nu}=\kappa^2T^{M}_{\mu\nu}+\kappa^2T^{SC}_{\mu\nu}, \tag{2.1}$$

with

$$T^{M}_{\mu\nu}=T^{SV}_{\mu\nu}+T^{NMC}_{\mu\nu}, \tag{2.2}$$

where $T^{SV}_{\mu\nu}$ represents the stress-energy tensor, which relates to the SVM. In addition, the information on the nonminimum coupling between the SC and the SVM is contained in the stress-energy tensor $T^{NMC}_{\mu\nu}$. $T^{SC}_{\mu\nu}$ in Eq. (2.1) denotes the stress-energy tensor of the SC, which reads

$$T^{SC}_{\mu\nu}=\frac{\rho\Sigma^{\alpha}_{\mu}\Sigma_{\alpha\nu}}{8\pi\sqrt{-\gamma}}, \tag{2.3}$$

where ρ denotes the density of the SC. $T^{SC}_{\mu\nu}$ is subject to the following conservation laws $\nabla_{\mu}T^{SC^{\mu\nu}}$ (see the Appendix). Rodrigues *et al.*, according to the Einstein equations, derive the nonrotating black hole mimicker surrounded by the SC [21]

$$ds^2=f(r)dt^2-g(r)^{-1}dr^2-\mathcal{R}^2\left(d\theta^2+\sin^2\theta d\phi^2\right), \tag{2.4}$$

and

$$f(r)=g(r)=1-L-\frac{2M}{\sqrt{\ell^2+r^2}},\qquad \mathcal{R}=\sqrt{\ell^2+r^2}, \tag{2.5}$$

where ℓ is a parameter responsible for central singularity regularization. If $\ell=0$, this spacetime metric will degenerate into the Letelier spacetime, and it will degenerate into the SVM when $L=0$. This spacetime have no event horizon for $L=1$, so that the SC parameters is limited to $0<L<1$. Moreover, the remarkable feature of this spacetime is that it can change from a black hole to a wormhole, so there is a threshold in the process of this transformation

$$\ell_c = \frac{2M}{\sqrt{1-2L+L^2}}. \tag{2.6}$$

As the parameter ℓ changes, the black bounce surrounded by the SC will represent various spacetime backgrounds: 1) when $0 < \ell < \ell_c$, the spacetime is regular black hole surrounded by the SC; 2) when $\ell = \ell_c$, the spacetime is one-way wormhole surrounded by the SC; 3) When $\ell > \ell_c$, the spacetime is traversable wormhole surrounded by the SC.

III. THE ROTATING BLACK HOLE MIMICKER SURROUNDED BY THE SC

In this section, we use the NJ method to obtain the rotating black hole mimicker surrounded by the SC. In the NJ method, it is usually necessary to solve a series of differential equations to obtain the Kerr-like black hole metric [61–63]. To obtain the spacetime metric of rotating black hole mimicker in a cloud of string, we first transform the spherically symmetric metric from Boyer-Lindquist to Eddington-Finkelstein coordinates. For this, we use the following coordinate transformation:

$$\mathrm{d}u = \mathrm{d}t - \frac{\mathrm{d}r}{\sqrt{f(r)g(r)}}. \tag{3.1}$$

After using this coordinate transformation, the spherically symmetric spacetime metric becomes

$$g^{\mu\nu} = -l^\mu n^\nu - l^\nu n^\mu + m^\mu \bar{m}^\nu + m^\nu \bar{m}^\mu, \tag{3.2}$$

where m is a complex vector, $\bar{m}$ is the complex conjugate of vector m, and vectors n and l are real. Moreover, the four basis vectors (l^μ, n^μ, m^μ and $\bar{m}^\mu$) satisfy the modulus of the basis vector to be 1 and the orthogonality conditions between the base vectors. For the metric of a rotating black bounce in a cloud of string, the basis vectors are

$$\begin{aligned} l^\mu &= \delta^\mu_r, \\ n^\mu &= \sqrt{\frac{g(r)}{f(r)}}\delta^\mu_\mu - \frac{f(r)}{2}\delta^\mu_r, \\ m^\mu &= \frac{1}{\sqrt{2}\mathcal{R}^2}\delta^\mu_\theta + \frac{i}{\sqrt{2}r\sin\theta}\delta^\mu_\phi, \\ \bar{m}^\mu &= \frac{1}{\sqrt{2}\mathcal{R}^2}\delta^\mu_\theta - \frac{i}{\sqrt{2}r\sin\theta}\delta^\mu_\phi. \end{aligned} \tag{3.3}$$

The spacetime coordinates between different observers satisfy the following complex transformation in the null trade,

$$u \to u - ia\cos\theta, \qquad r \to r - ia\cos\theta. \tag{3.4}$$

When using this transformation, the metric coefficients become more complex functions of the (r, θ, a). After using this transformation, the metric functions change as follows: $f(r) \to \mathcal{F}(r, \theta, a)$, $g(r) \to \mathcal{G}(r, \theta, a)$ and $h(r) \to \Sigma(r, \theta, a)$. One can find that the original form can be recovered by setting $a = 0$. Moreover, the null tetrad after using the complex transformation become

$$\begin{aligned} l^\mu &= \delta^\mu_r, \\ n^\mu &= \sqrt{\frac{\mathcal{G}}{\mathcal{F}}}\delta^\mu_\mu - \frac{\mathcal{F}}{2}\delta^\mu_r, \\ m^\mu &= \frac{1}{\sqrt{2\Sigma}}\left[\delta^\mu_\theta + ia\sin\theta(\delta^\mu_u - \delta^\mu_r) + \frac{i}{\sin\theta}\delta^\mu_\phi\right], \\ \bar{m}^\mu &= \frac{1}{\sqrt{2\Sigma}}\left[\delta^\mu_\theta - ia\sin\theta(\delta^\mu_u - \delta^\mu_r) - \frac{i}{\sin\theta}\delta^\mu_\phi\right]. \end{aligned} \tag{3.5}$$

Therefore, according to the expression of the inverse metric (3.2), we can obtain the contravariant nonzero metric components of a rotating black bounces in a cloud of string

$$\begin{aligned} &g^{uu} = \frac{a^2\sin^2\theta}{\Sigma}, \qquad g^{ur} = -\sqrt{\frac{\mathcal{G}}{\mathcal{F}}} - \frac{a^2\sin^2\theta}{\Sigma}, \\ &g^{rr} = \mathcal{F} + \frac{a^2\sin^2\theta}{\Sigma}, \qquad g^{r\phi} = -\frac{a}{\Sigma}, \qquad g^{\theta\theta} = \frac{1}{\Sigma}, \\ &g^{\phi\phi} = \frac{1}{\Sigma\sin^2\theta}, \qquad g^{u\phi} = \frac{a}{\Sigma}. \end{aligned} \tag{3.6}$$

The covariant nonzero components can be read as

$$\begin{aligned} &g_{uu} = -\mathcal{F}, g_{ur} = -\sqrt{\frac{\mathcal{F}}{\mathcal{G}}}, \qquad g_{u\phi} = a\sin^2\theta\left(\mathcal{F} - \sqrt{\frac{\mathcal{G}}{\mathcal{F}}}\right), \\ &g_{r\phi} = a\sin^2\theta\sqrt{\frac{\mathcal{F}}{\mathcal{G}}}, \qquad g_{\theta\theta} = \Sigma, \\ &g_{\phi\phi} = \Sigma\sin^2\theta + a^2\left(2\sqrt{\frac{\mathcal{G}}{\mathcal{F}}} - \mathcal{F}\right)\sin^4\theta. \end{aligned} \tag{3.7}$$

Therefore, we can obtain the rotating black bounces in a cloud of string under Eddington-Finkelstein coordinates

$$\begin{aligned} ds^2 = &-\mathcal{F}du^2 - 2\sqrt{\frac{\mathcal{F}}{\mathcal{G}}}dudr + 2a\sin^2\theta\left(\mathcal{F} - \sqrt{\frac{\mathcal{G}}{\mathcal{F}}}\right)dud\phi \\ &+ 2a\sin^2\theta\sqrt{\frac{\mathcal{F}}{\mathcal{G}}}drd\phi + \Sigma d\theta^2 \\ &+ \left[\Sigma\sin^2\theta + a^2\left(2\sqrt{\frac{\mathcal{G}}{\mathcal{F}}} - \mathcal{F}\right)\sin^4\theta\right]d\phi^2. \end{aligned} \tag{3.8}$$

From a physical point of view, we need to transform the Eddington-Finkelstein coordinates back to Boyer-Lindquist coordinates. The corresponding coordinate transformation is

$$du = dt + \lambda_1(r)dr, \qquad d\phi = d\phi + \lambda_2(r)dr, \tag{3.9}$$

where the transformation functions $\lambda_1(r)$ and $\lambda_2(r)$ can use this form [16]

$$\lambda_1(r) = -\frac{\mathcal{K}(r)+a^2}{g(r)h(r)+a^2}, \qquad \lambda_2(r) = -\frac{a}{g(r)h(r)+a^2}, \tag{3.10}$$

where

$$\mathcal{K}(r) = \sqrt{\frac{g(r)}{f(r)}}h(r), \tag{3.11}$$

and

$$\mathcal{F}(r,\theta) = \frac{(gh+a^2\cos^2\theta)\Sigma}{(\mathcal{K}+a^2\cos^2\theta)^2}, \qquad \mathcal{G}(r,\theta) = \frac{gh+a^2\cos^2\theta}{\Sigma}. \tag{3.12}$$

Therefore, we obtain the line element of the rotating black hole mimicker surrounded by the string cloud

$$\begin{aligned} ds^2 = &-\left[1-\frac{L(r^2+\ell^2)+2M\sqrt{r^2+\ell^2}}{\Sigma}\right]dt^2+\frac{\Sigma}{\Delta}dr^2 \\ &+\Sigma d\theta^2-\frac{2a\left[2M\sqrt{r^2+\ell^2}+L(r^2+\ell^2)\right]\sin^2\theta}{\Sigma}dt\,d\phi \\ &+\frac{A\sin^2\theta}{\Sigma}d\phi^2 \end{aligned} \tag{3.13}$$

with

$$\begin{aligned} \Sigma &= r^2+\ell^2+a^2\cos^2\theta, \\ \Delta &= r^2+\ell^2+a^2-\left[2M\sqrt{r^2+\ell^2}+L(r^2+\ell^2)\right], \\ A &= (r^2+\ell^2+a^2)^2-\Delta a^2\sin^2\theta. \end{aligned} \tag{3.14}$$

When $a=0$, the rotating black bounces in a cloud of string can degenerate into nonrotating black bounces in a cloud of string [21]. When $L=0$, the rotating black bounces in a cloud of string can degenerate into the rotating black hole mimickers [13]. Moreover, the rotating black bounces in a cloud of string can degenerate into Kerr black hole metric when $L=0, \ell=0$.

IV. GEODESICS AROUND THE ROTATING BLACK HOLE MIMICKER SURROUNDED BY THE STRING CLOUD

The photons emitted from infinity will generally have two completely different endings when they pass through a black hole; the photon with a larger orbital angular momentum will be detected by an observer at infinity when it passes through some turning points and the second outcome is that photons with smaller orbital angular momentum will fall into the black hole due to the strong gravity of the black hole. We will study the geodesic equation of photons based on the spacetime metric of the rotating black hole mimicker surrounded by the SC. To do this, we will solve the Hamilton-Jacobi equation, which can be written as

$$\frac{\partial S}{\partial \lambda} = -H, \tag{4.1}$$

where S represents the Jacobi action, and λ represents the affine parameter of the geodesic. Moreover, the Hamiltonian can be given by

$$H = \frac{1}{2}g^{\mu\nu}\frac{\partial S}{\partial x^\mu}\frac{\partial S}{\partial x^\nu}. \tag{4.2}$$

In the GR, the Hamilton-Jacobi equation can be read as

$$\frac{\partial S}{\partial \lambda} = -\frac{1}{2}g^{\mu\nu}\frac{\partial S}{\partial x^\mu}\frac{\partial S}{\partial x^\nu}. \tag{4.3}$$

To separate variables for geodesic equations, we use the separability ansatz

$$S = \frac{1}{2}\mu^2\lambda - Et + \mathcal{L}\phi + S_r(r) + S_\theta(\theta) \tag{4.4}$$

with the particle mass μ. The two conserved quantities in photon motion are E and $\mathcal{L}$. Moreover, $S_r(r)$ and $S_\theta(\theta)$ represent radial and angular functions, respectively. Based on these two conserved quantities and unknown functions $[S_r(r)$ and $S_\theta(\theta)]$, we can substitute action S into the Hamilton-Jacobi equation (4.3) to obtain the following four equations

$$\begin{aligned} \Delta\Sigma\frac{dt}{d\lambda} &= A - a\frac{\mathcal{L}}{E}\left[2M\sqrt{r^2+\ell^2}+L(r^2+\ell^2)\right], \\ \Sigma\frac{dr}{d\lambda} &= \sqrt{R(r)}, \\ \Sigma\frac{d\theta}{d\lambda} &= \sqrt{\Theta(\theta)}, \\ \Sigma\frac{d\phi}{d\lambda} &= \frac{a}{\Delta}\left(E(r^2+\ell^2+a^2)-a\mathcal{L}\right)-\left(aE-\frac{\mathcal{L}}{\sin^2\theta}\right), \end{aligned} \tag{4.5}$$

where the $R(r)$ and $\Theta(\theta)$ can be read as

$$\begin{aligned} R(r) &= \left[E(r^2+\ell^2+a^2)-a\mathcal{L}\right]^2-\Delta\left[\mathcal{Q}+(\mathcal{L}-aE)^2\right], \\ \Theta(\theta) &= \mathcal{Q}+a^2E^2\cos^2\theta-\mathcal{L}^2\cot^2\theta, \end{aligned} \tag{4.6}$$

where $\mathcal{Q}$ is Carter constant [64], which is the integral constant for the geodesic motion of photons in a rotating

black hole spacetime. $R(r)$ and $\Theta(\theta)$ to the photon motion must be greater than 0, so there are

$$\frac{R(r)}{E^2} = \left[r^2 + \ell^2 + a^2 - a\xi\right]^2 - \Delta(r)\left[\eta + (\xi - a)^2\right] \geq 0, \tag{4.7}$$

$$\frac{\Theta(\theta)}{E^2} = \eta + (\xi - a)^2 - \left(\frac{\xi}{\sin\theta} - a\sin\theta\right)^2 \geq 0. \tag{4.8}$$

Among them, the collision parameters determined the photon motion are defined as $\xi = \mathcal{L}/E$ and $\eta = \mathcal{Q}/E^2$. Since a black hole has an event horizon, light cannot escape from its surface, so some one may think that the size of the black hole shadow seen is determined by the black hole event horizon. In fact, there is a special surface outside the event horizon of the black hole, namely the photosphere. When a photon enters the photosphere, it will be captured by the black hole, so it cannot reach the observer at infinity. Only light rays that are outside the photosphere can reach the observer. Therefore, the boundary and size of the black hole shadow actually depend on the size of the photosphere. In general rotating black hole spacetime, the orbit of the photosphere must satisfy $R(r_{ph}) = 0, R'(r_{ph}) = 0$, $R''(r_{ph}) \geq 0$, where r_{ph} is the radius of the unstable photosphere. According to the first two conditions, we can get critical impact parameters

$$\xi = \frac{-\left((\ell^2 + r^2)(3M + (L-1)\sqrt{\ell^2 + r^2})\right) + a^2(M + (1+L)\sqrt{\ell^2 + r^2})}{a(M + (L-1)\sqrt{\ell^2 + r^2})}, \tag{4.9}$$

and

$$\eta = \frac{-(\ell^2 + r^2)}{a^2(M + (L-1)\sqrt{\ell^2 + r^2})^2}\Big[\ell^4(L-1)^2 + 9M^2r^2 + (L-1)^2r^4 + 2M\sqrt{\ell^2 + r^2}\left(-2a^2 + 3(L-1)r^2\right) + \ell^2(9M^2 + 2(L-1)^2r^2 + 6(L-1)M\sqrt{\ell^2 + r^2})\Big]. \tag{4.10}$$

V. THE SHADOW OF ROTATING BLACK HOLE MIMICKER SURROUNDED BY THE STRING CLOUD

In the previous section we calculate the geodesics of photon motion. Based on the geodesics we can study the photon motion in the rotating black bounces surrounded by the SC measured by the observer. To facilitate the calculation of shadow images, the general approach is to use the celestial coordinates α and β. This coordinate is on the celestial plane perpendicular to the line connecting the observer to the center of spacetime. For an observer at (r_0, θ_0), the celestial coordinates can be written as [65]

$$\alpha = \lim_{r_0\to\infty}\left(-r_0^2\sin\theta_0\frac{d\phi}{dr}\right), \tag{5.1}$$

and

$$\beta = \lim_{r_0\to\infty}\left(r_0^2\frac{d\theta}{dr}\right), \tag{5.2}$$

where r_0 is the distance from the observer to the black hole, and θ_0 is the angle between the line connecting the observer to the center of the black hole and the rotation axis of the black hole. For asymptotically flat spacetime metrics, the celestial coordinates can be reduced to

$$\alpha = -\frac{\xi}{\sin\theta_0}, \tag{5.3}$$

and

$$\beta = \pm\sqrt{\eta + a^2\cos^2\theta_0 - \xi^2\cot^2\theta_0}. \tag{5.4}$$

For our rotating black hole mimicker surrounded by the SC, when $\theta_0 = \pi/2$, the celestial coordinates can be written as

$$\alpha = -\frac{a^2\left(M + (1+L)\sqrt{\ell^2 + r^2}\right) - \left((\ell^2 + r^2)(3M + (L-1)\sqrt{\ell^2 + r^2})\right)}{a(M + (L-1)\sqrt{\ell^2 + r^2})}, \tag{5.5}$$

and

$$\beta = \pm\Bigg\{-\frac{(\ell^2 + r^2)}{a^2(M + (L-1)\sqrt{\ell^2 + r^2})^2}\Big[\ell^4(L-1)^2 + 9M^2r^2 + (L-1)^2r^4 + 2M\sqrt{\ell^2 + r^2}\left(3(L-1)r^2 - 2a^2\right) + \ell^2\left(9M^2 + 2(L-1)^2r^2 + 6(L-1)M\sqrt{\ell^2 + r^2}\right)\Big]\Bigg\}^{1/2}. \tag{5.6}$$

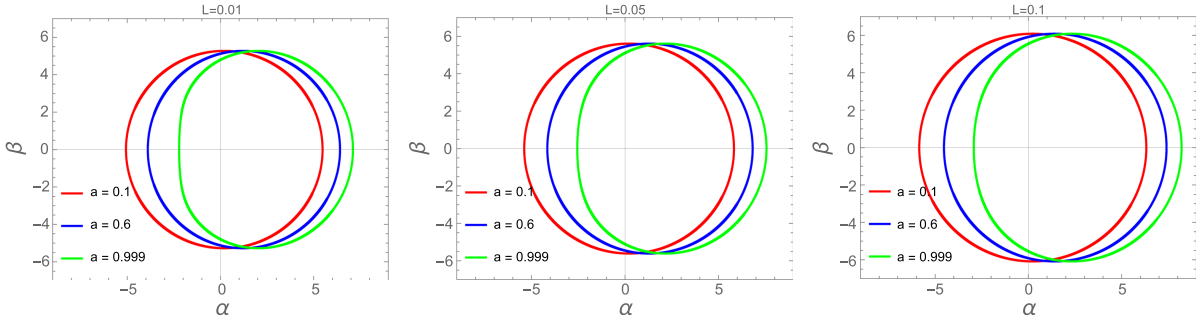

FIG. 1. The shape of the shadow of the rotating black hole mimicker surrounded by the SC for different a with $M = 1, \ell = 0.1$. The values of L from left to right are 0.01, 0.05, 0.1, respectively.

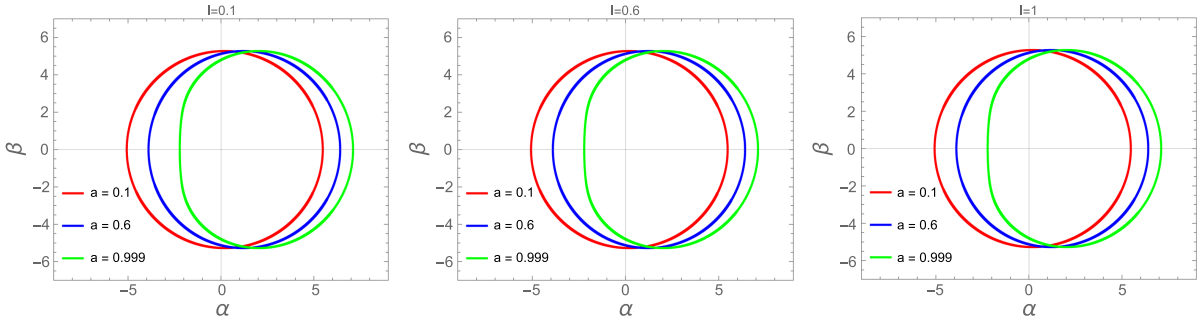

FIG. 2. The shape of the shadow of the rotating black hole mimicker surrounded by the SC for different a with $M = 1, L = 0.01$. The values of ℓ from left to right are 0.1, 0.6, 1, respectively.

Now we can use Eqs. (5.5) and (5.6) to calculate the shadow of rotating metric surrounded by the SC, so that we can study the influence of the SC on the rotating black hole mimicker.

We first study the effect of the spin parameter a on the shadow of the rotating black hole mimicker surrounded by the SC. Figure 1 gives the shape of the shadow of the rotating black hole mimicker surrounded by the SC for different a with $M = 1, \ell = 0.1$, where values of L from left to right are 0.01, 0.05, 0.1, respectively. Figure 1 gives the shape of the shadow of the rotating black hole mimicker surrounded by the SC for different a with $M = 1$, $L = 0.01$, where values of ℓ from left to right are 0.1, 0.6, 1, respectively. From Fig. 1 and Fig. 2, we can see that when the spin parameter is small, the shape of the shadow is closer to a circle with a fixed radius, but when the spin parameter is larger, the shape of the shadow is deformed. That is, the increase of the spin parameter a makes the shape of the shadow present a D-shaped feature. The reason for this deformation is that in the high-speed rotating black bounces spacetime surrounded by the SC, due to the drag effect brought by its rotation, the unstable circular orbits of prograde and retrograde photons are no longer symmetrical, so that the shadow is a D-shape for the equatorial plane observer.

On the other hand, in Fig. 3 we study the effect of the SC parameter L on the shape of the shadow of the rotating

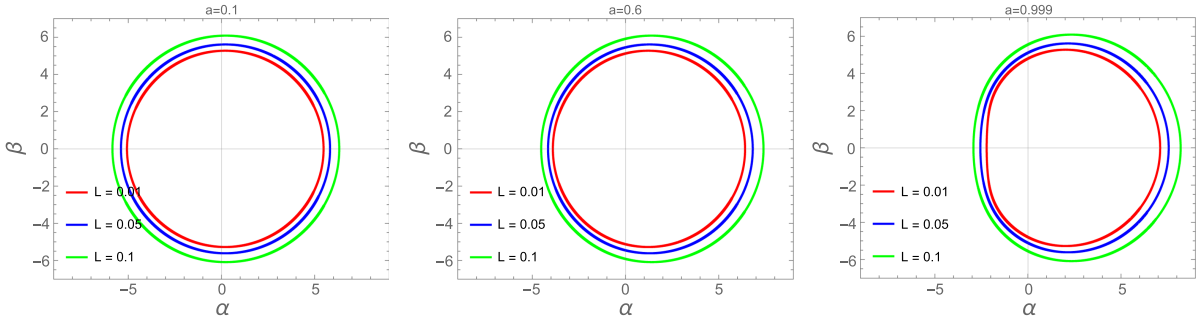

FIG. 3. The shape of the shadow of the rotating black hole mimicker surrounded by the SC for different L with $M = 1, \ell = 0.1$. The values of a from left to right are 0.1, 0.6, 0.999, respectively.

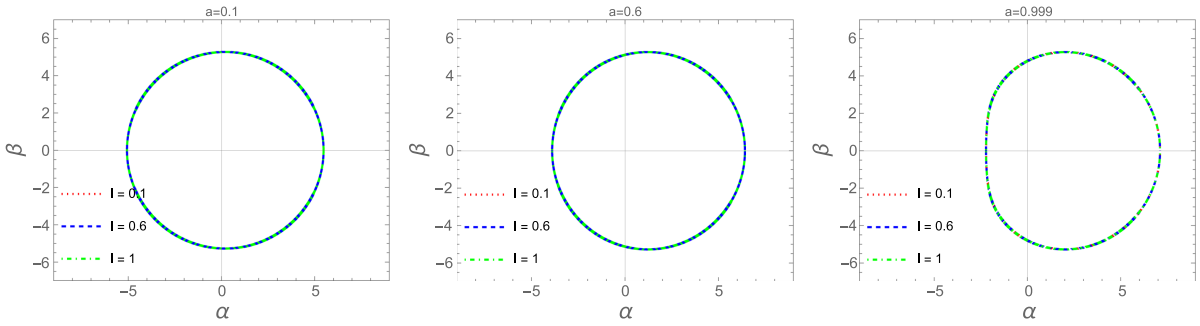

FIG. 4. The shape of the shadow of the rotating black hole mimicker surrounded by the SC for different ℓ with $M = 1, L = 0.01$. The values of a from left to right are 0.1, 0.6, 0.999, respectively.

black hole mimicker surrounded by the SC, where $M = 1, \ell = 0.1$, and the values of a from left to right are 0.1, 0.6, 0.999, respectively. One can see that when the SC parameter is gradually increased from $L = 0.01$, the boundary of the black bounce shadow is continuously increasing, which is consistent for different spin parameters. But when the spin parameter a is small, for example $a = 0.1$, the shape of the shadow is closer to the standard circle. From the shadow of the spin parameter $a = 0.999$, it can be seen that the shadow at this time becomes a D-shape again. But for a larger SC parameter $L = 0.1$, the shape of the shadow is not as close to a D-shape as the shadow of $L = 0.01$. Therefore, our results show that the SC have a significant impact on black bounce shadows, both in size and shape. In Fig. 4 we investigate the influence of the parameter ℓ responsible for central singularity regularization on shadow. From Fig. 4, we can see that the red dotted line represents the shadow image of $\ell = 0.1$, the blue dotted line represents the shadow image of $\ell = 0.6$, and the green dotted line represents $\ell = 1$ shaded image. One can see that an increase in ℓ has such a small effect on the shadow that we see that the shadows corresponding to different ℓ almost coincide. But when the spin a is larger, the D-shaped shadow image still appears. In addition, we have verified that when ℓ is larger than a critical value (i.e., the spacetime line element (3.13) represents a traversable wormhole spacetime), the result shows a similar behavior to the shadow image when the spacetime line element represents a black hole spacetime. This demonstrates that we cannot distinguish whether the rotating black hole mimicker surrounded by the SC is a black hole or a wormhole through the shadow.

VI. RADIUS AND DISTORTION OF THE SHADOW AND ENERGY EMISSION RATE

The radius of the shadow and the distortion are two important observables. Here we will study the radius of the shadow and the distortion of the rotating black hole mimicker surrounded by the string cloud. The shadow radius (R_s) describes the scale of the black hole's shadow shape. The distortion (δ_s) of the shadow describes how far the boundary of the black hole's shadow deviates from the standard circle. Their specific mathematical expression is [66,67]

$$R_s = \frac{(\alpha_t - \alpha_r)^2 + \beta_t^2}{2|\alpha_r - \alpha_t|}, \tag{6.1}$$

$$\delta_s = \frac{|\alpha_p - \tilde{\alpha}_p|}{R_s}. \tag{6.2}$$

More details of radius and distortion are presented in Ref. [65]. From Fig. 5, one can see that the shadow radius

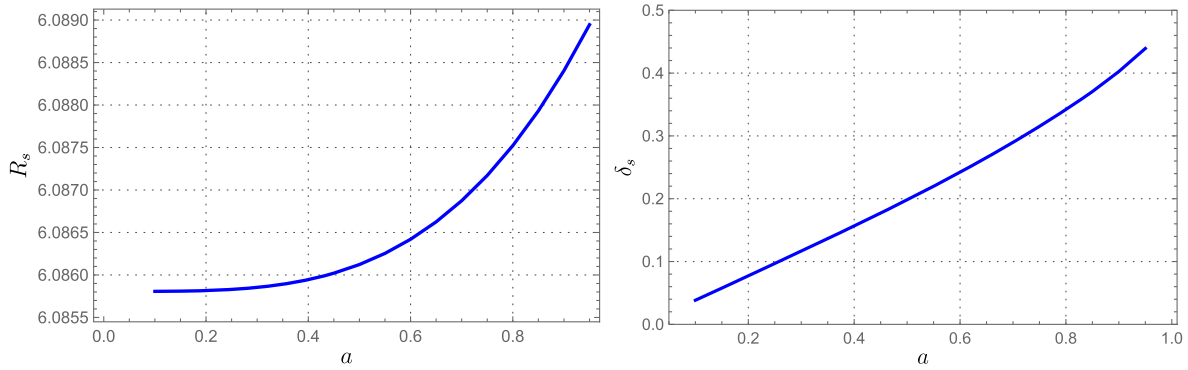

FIG. 5. The radius (left panel) and distortion (right panel) of the shadow as the function of the spin a with $M = 1, \ell = 0.1, L = 0.1$.

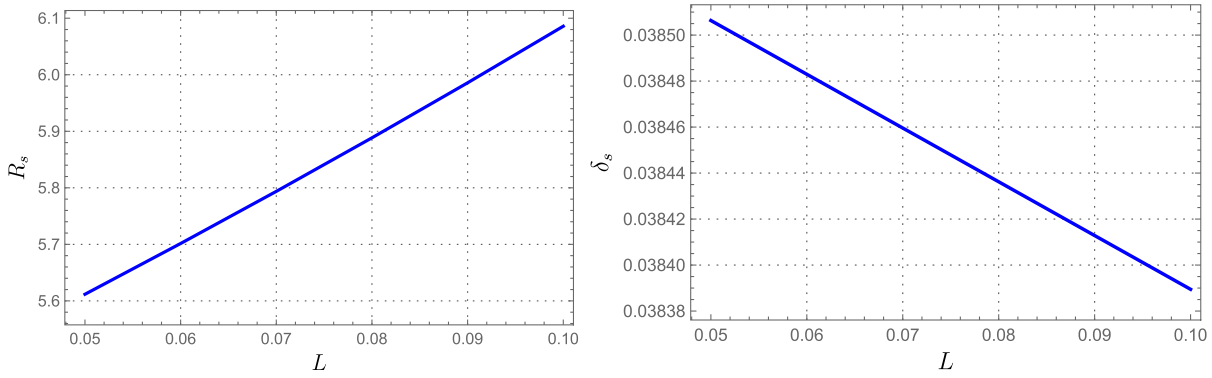

FIG. 6. The radius (left panel) and distortion (right panel) of the shadow as the function of L with $M = 1, \ell = 0.1, a = 0.1$.

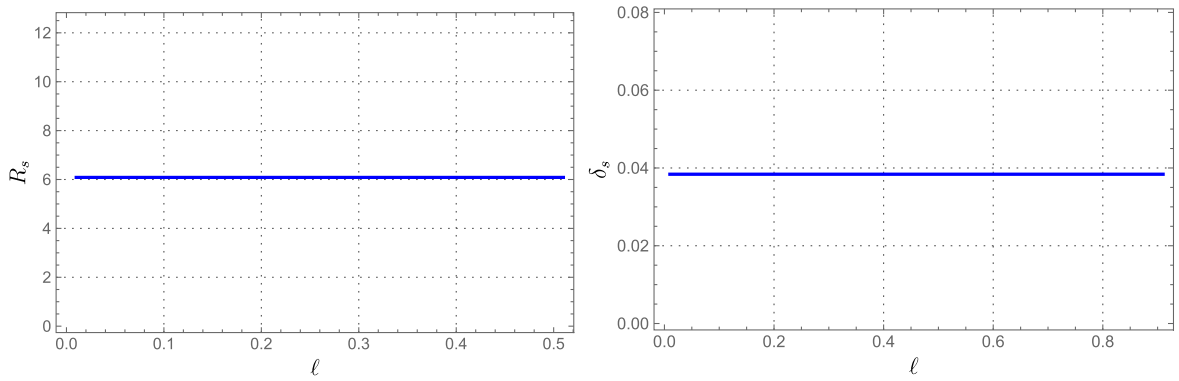

FIG. 7. The radius (left panel) and distortion (right panel) of the shadow as the function of ℓ with $M = 1, L = 0.1, a = 0.1$.

R_s increases slowly when a is small and increases sharply when a is large as spin a increases. We can also see that as spin a increases, the distortion δ_s of rotating black hole mimicker surrounded by the string cloud increases significantly. Therefore, the shadow of the rotating black hole mimicker surrounded by the string cloud takes on a distinct D-shape when a is large. Furthermore, from Fig. 6 we can see that the radius R_s of the shadow increases sharply as L increases. The distortion δ_s decreases as L increases. In Fig. 7 we give the radius and distortion of the shadow as the function of ℓ. Figure 7 shows that the shadow radius R_s and shadow distortion δ_s remain almost unchanged as ℓ increases. That is, as ℓ changes, the radius of the shadow hardly changes, and there is no significant distortion. These notable features of the rotating black hole mimicker surrounded by the string cloud's shadow radius R_s and shadow distortion δ_s make it possible to be detected by EHT observations.

For an observer at infinity, the area of the black hole's shadow is very close to the high-energy absorption cross-section (Ω). In a spherically symmetric black hole, the absorption section fluctuates at Ω. For the shadow with the radius of R_s, we have $\Omega \approx \pi R_s^2$. The energy emission rate of the black hole can be given by

$$\frac{d^2E(\omega)}{d\omega dt} = \frac{2\pi^2\omega^3\Omega}{e^{\frac{\omega}{T}} - 1}, \tag{6.3}$$

where ω denotes the frequency of the photon and T denotes the Hawking temperature at the event horizon of the rotating black hole mimicker surrounded by the string cloud, which can be given by [66]

$$T = \lim_{\theta\to 0, r\to r_+} \frac{1}{2\pi\sqrt{g_{rr}}} \frac{\partial\sqrt{g_{tt}}}{\partial r}. \tag{6.4}$$

In Figs. 8 and 9, we give the energy emission rate as the function of the particle frequency ω. We can see that the peak of the energy emission rate gradually decreases as the spin a increases. The peak of the energy emission rate increases as ℓ increases. Moreover, one can see that the peak of the energy emission rate decreases as L increases when a is small, but increases as L increases when a is large. This feature opens up new possibilities for the EHT to detect the rotating black hole mimicker surrounded by the string cloud.

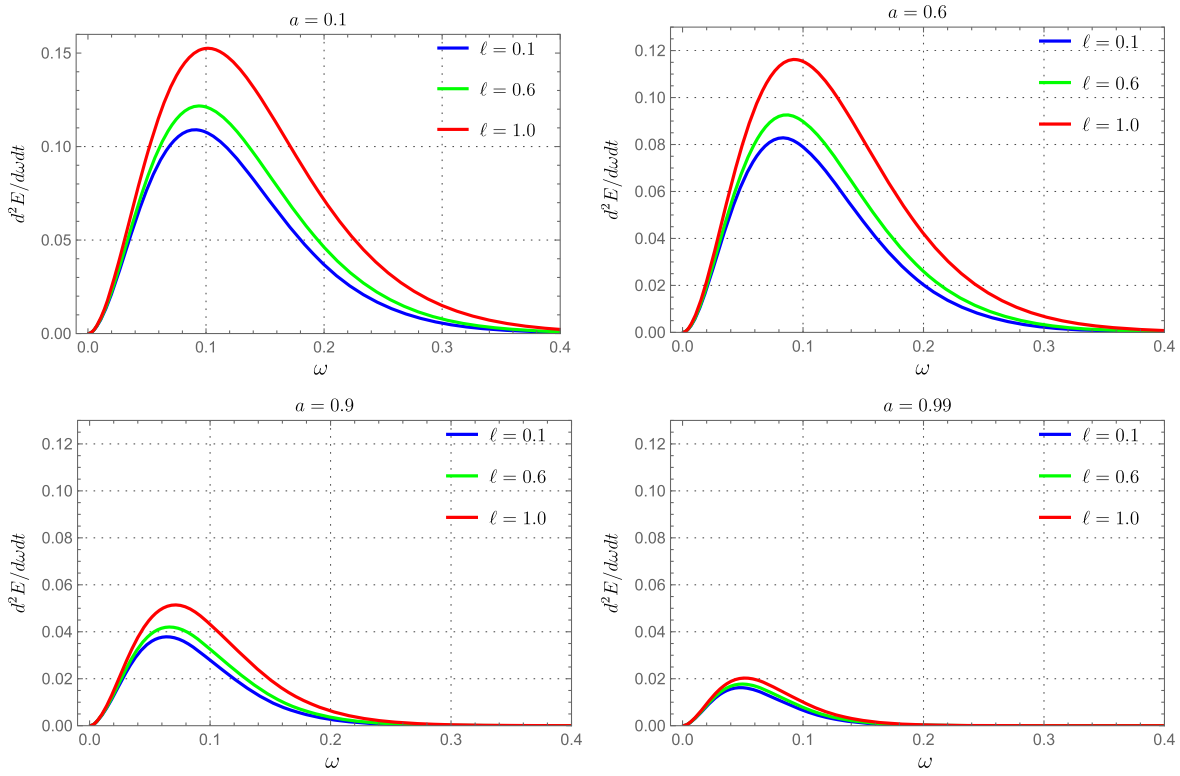

FIG. 8. The energy emission rate as the function of the particle frequency ω for different ℓ with $M = 1$, $L = 0.1$.

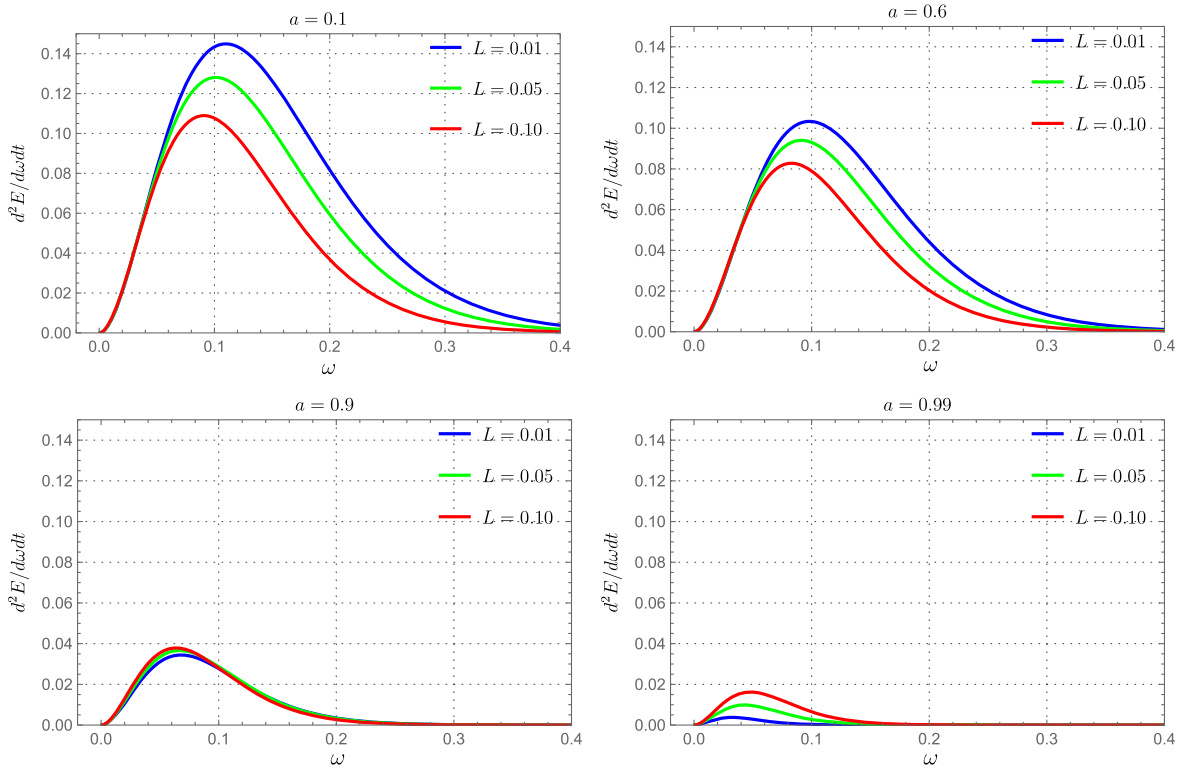

FIG. 9. The energy emission rate as the function of the particle frequency ω for different L with $M = 1, \ell = 0.1$.

VII. CONCLUSION

In this work, we first derive a rotating black hole mimicker surrounded by the SC using the Newman-Janis method. This rotating metric can be interpolated to represent regular black hole spacetime and wormhole spacetime. In this spacetime background, the Hamilton-Jacobi equation is solved to obtain the corresponding geodesic equation. Then we give the shadow image of this spacetime. We find that as the spin parameter a increases, the shadow gradually takes on a distinct D-shape. In addition, the SC parameter L has a remarkable effect on the shadow, and the increase of L sharply increases the boundary of the shadow, and also makes the D-shaped shadow closer to a circle. String cloud has a very significant contribution to the shadows of the rotating black hole mimicker surrounded by the string cloud, which makes string cloud expected to be detected by EHT. Our results show that the parameter l responsible for the central singularity regularization has a very weak influence on the shadow, so that we cannot use the shadow to distinguish whether the rotating black hole mimicker surrounded by the SC are the regular black holes or the wormholes. In Ref. [68], we studied the quasinormal modes of nonrotating black hole mimicker surrounded by the SC, and we found that the gravitational wave echoes appeared after the initial ringdown in this spacetime. It is very interesting to verify whether the rotating black hole mimicker surrounded by the SC will also appear gravitational wave echoes as expected in the next work. If so, the combination of shadow and gravitational wave echoes detection can help us determine whether this rotating spacetime is a black hole or a wormhole.

ACKNOWLEDGMENTS

This research was funded by the National Natural Science Foundation of China (No. 12265007 and No. 12261018), Universities Key Laboratory of System Modeling and Data Mining in Guizhou Province (No. 2023013), the Science and Technology Foundation of Guizhou Province (No. ZK[2022]YB029). The work of G. L. is supported by the Italian Istituto Nazionale di Fisica Nucleare (INFN) through the "QGSKY" project and by Ministero dell'Istruzione, Università e Ricerca (MIUR). G. L., and A. Ö. would like to acknowledge networking support by the COST Action CA18108—Quantum gravity phenomenology in the multimessenger approach (QG-MM). A. Ö. would like to acknowledge networking support by the COST Action CA21106—COSMIC WISPers in the Dark Universe: Theory, astrophysics and experiments (CosmicWISPers).

APPENDIX: STRING CLOUD MODEL

In this appendix, we review the main features of spacetimes in the presence of a cloud of strings, working in the framework of general relativity. The basic idea underlying the string model is that a string is associated with a world sheet (in analogy to a particle which is associated with a world line), which is described by $x^\mu(\lambda^A)$, where λ^0 and λ^1 are timelike and spacelike parameters. General relativity minimally coupled with matter and the cloud of strings is described by the total action

$$S = S_{GR} + S_M + S_{CS}, \tag{A1}$$

where $S_{GR} = \int d^4x\sqrt{-g}R$ is the Hilbert-Einstein action, S_M is the matter action, and S_{CS} is the Nambu-Goto action that describes stringlike objects, whose expression is given by [18]

$$S_{CS} = \mathcal{M}\int \sqrt{-\gamma}d\lambda^0 d\lambda^1. \tag{A2}$$

In (A2), $\mathcal{M}$ is a dimensionless constant characterizing the string, while $\gamma = \det\gamma_{AB}$, with γ_{AB} the induced metric on a submanifold defined as

$$\gamma_{AB} = g_{\mu\nu}\frac{\partial x^\mu}{\partial\lambda^A}\frac{\partial x^\nu}{\partial\lambda^B}, \qquad \lambda^A = 0, 1. \tag{A3}$$

The Nambu-Goto action can be rewritten as

$$S_{CS} = \int \mathcal{M}\left(-\frac{1}{2}\Sigma^{\mu\nu}\Sigma_{\mu\nu}\right)^{1/2} d\lambda^0 d\lambda^1, \tag{A4}$$

where $\Sigma^{\mu\nu}$ is the bivector defined as

$$\Sigma^{\mu\nu} = \epsilon^{AB}\frac{\partial x^\mu}{\partial\lambda^A}\frac{\partial x^\nu}{\partial\lambda^B}, \tag{A5}$$

being ϵ^{AB} the Levi-Civita symbol with nonvanishing components given by $\epsilon^{01} = -\epsilon^{10} = 1$. The variation of the action (A1) with respect to the metric tensor gives the field equations (2.1), where $T^M_{\mu\nu}$ is the usual stress-energy tensor of the matter, and $T^{CS}_{\mu\nu}$ the stress-energy tensor of the string cloud, given by (2.3) [18]. Moreover, the stress-energy tensor $T^{CS}_{\mu\nu}$ satisfies the conservation law

$$\begin{aligned}\nabla_\mu T^{CS\mu\nu} &= \nabla_\mu\left(\frac{\rho\Sigma^{\mu\alpha}\Sigma_\alpha{}^\nu}{8\pi\sqrt{-\gamma}}\right)\\ &= \nabla_\mu(\rho\Sigma^{\mu\alpha})\frac{\Sigma_\alpha{}^\nu}{8\pi\sqrt{-\gamma}} + \rho\Sigma^{\mu\alpha}\nabla_\mu\left(\frac{\Sigma_\alpha{}^\nu}{8\pi\sqrt{-\gamma}}\right) = 0.\end{aligned} \tag{A6}$$

1. Simpson-Visser solution with the cloud of strings

The standard Simpson-Visser (SV) solution is characterized by the fact that it describes a regular black hole (and, depending on the parameters of the metric, it can describe a wormhole). To obtain the SV solution in the presence of a

cloud of string, the energy-momentum tensor $T_{\mu\nu}{}^{M}$ in (2.1) is given by (2.2). The nonvanishing components of the stress-energy tensor $T^{SV}_{\mu\nu}$, associated with the SV solution, are [10]

$$T^{SV}_{00} = -\frac{l^2\left(\sqrt{l^2+r^2}-4M\right)\left(\sqrt{l^2+r^2}-2M\right)}{8\pi(l^2+r^2)^3}, \qquad T^{SV}_{11} = \frac{l^2}{8\pi(l^2+r^2)^{3/2}(2M-\sqrt{l^2+r^2})},$$
$$T^{SV}_{22} = \frac{l^2\left(\sqrt{l^2+r^2}-M\right)}{8\pi(l^2+r^2)^{3/2}}, \qquad T^{SV}_{33} = \frac{l^2\sin^2\theta\left(\sqrt{l^2+r^2}-M\right)}{8\pi(l^2+r^2)^{3/2}}. \tag{A7}$$

The nonvanishing components of the stress-energy tensor $T^{NMC}_{\mu\nu}$, which provides information about the nonminimal coupling between the SV metric and the cloud of string, are

$$T^{NMC}_{00} = -\frac{Ll^2\left((L-2)\sqrt{l^2+r^2}+6M\right)}{8\pi(l^2+r^2)^{5/2}},$$
$$T^{NMC}_{11} = \frac{2Ll^2M}{8\pi(l^2+r^2)^{3/2}(\sqrt{l^2+r^2}-2M)\left((L-1)\sqrt{l^2+r^2}+2M\right)},$$
$$T^{NMC}_{22} = -\frac{Ll^2}{8\pi(l^2+r^2)}, \qquad T^{CP}_{33} = -\frac{Ll^2\sin^2\theta}{8\pi(l^2+r^2)}. \tag{A8}$$

Notice that for $L=0$ or $l=0$ all the components of $T^{NMC}_{\mu\nu}$ vanish.

Finally, the nonvanishing components of the cloud of strings $T^{CS}_{\mu\nu}$ are

$$T^{CS0}{}_{0} = T^{CS1}{}_{1} = \frac{L}{8\pi(r^2+l^2)}. \tag{A9}$$

To guarantee the positivity of the energy density it is required $L>0$. By using Eqs. (2.1) and (A7), (A8), and (A9) one infers a set of equations leading to metric function (2.5).

[1] K. Schwarzschild, On the gravitational field of a mass point according to Einstein's theory, Sitzungsber. Preuss. Akad. Wiss. Berlin (Math. Phys.) **1916**, 189 (1916).

[2] R. P. Kerr, Gravitational field of a spinning mass as an example of algebraically special metrics, Phys. Rev. Lett. **11**, 237 (1963).

[3] P. S. Joshi, Gravitational collapse: The story so far, Pramana **55**, 529 (2000).

[4] N. Tsukamoto, Gravitational lensing in the Simpson-Visser black-bounce spacetime in a strong deflection limit, Phys. Rev. D **103**, 024033 (2021).

[5] J. Barrientos, A. Cisterna, N. Mora, and A. Viganò, AdS-Taub-NUT spacetimes and exact black bounces with scalar hair, Phys. Rev. D **106**, 024038 (2022).

[6] A. Övgün, Weak deflection angle of black-bounce traversable wormholes using Gauss-Bonnet theorem in the dark matter medium, Turk. J. Phys. **44**, 465 (2020).

[7] A. Övgün, Weak field deflection angle by regular black holes with cosmic strings using the Gauss-Bonnet theorem, Phys. Rev. D **99**, 104075 (2019).

[8] M. Calzá, Evaporation of a Kerr-black-bounce by emission of scalar particles, Phys. Rev. D **107**, 044067 (2023).

[9] J. Bardeen, Non-singular general relativistic gravitational collapse, in *Proceeding of the International Conference GR5, Tbilisi, USSR, Georgia* (1968), p. 174, https://ui.adsabs.harvard.edu/abs/1968qtr..conf...87B.

[10] A. Simpson and M. Visser, Black-bounce to traversable wormhole, J. Cosmol. Astropart. Phys. 02 (2019) 042.

[11] K. Pal, K. Pal, P. Roy, and T. Sarkar, Regularizing the JNW and JMN naked singularities, Eur. Phys. J. C **83**, 397 (2023).

[12] K. Pal, K. Pal, R. Shaikh, and T. Sarkar, A rotating modified JNW spacetime as a Kerr black hole mimicker, arXiv:2305.07518.

[13] J. Mazza, E. Franzin, and S. Liberati, A novel family of rotating black hole mimickers, J. Cosmol. Astropart. Phys. 04 (2021) 082.

[14] E. T. Newman and A. I. Janis, Note on the Kerr spinning particle metric, J. Math. Phys. (N.Y.) **6**, 915 (1965).

[15] M. Azreg-Ainou, Regular and conformal regular cores for static and rotating solutions, Phys. Lett. B **730**, 95 (2014).

[16] M. Azreg-Aïnou, Generating rotating regular black hole solutions without complexification, Phys. Rev. D **90**, 064041 (2014).
[17] R. Shaikh, K. Pal, K. Pal, and T. Sarkar, Constraining alternatives to the Kerr black hole, Mon. Not. R. Astron. Soc. **506**, 1229 (2021).
[18] P. S. Letelier, Clouds of strings in general relativity, Phys. Rev. D **20**, 1294 (1979).
[19] P. S. Letelier, String Cosmologies, Phys. Rev. D **28**, 2414 (1983).
[20] S. K. Jha and A. Rahaman, Superradiance scattering off rotating Simpson-Visser black hole and its shadow in the non-commutative setting, arXiv:2208.13176.
[21] M. E. Rodrigues and M. V. d. S. Silva, Embedding regular black holes and black bounces in a cloud of strings, Phys. Rev. D **106**, 084016 (2022).
[22] H. H. Soleng, Dark matter and nonNewtonian gravity from general relativity coupled to a fluid of strings, Gen. Relativ. Gravit. **27**, 367 (1995).
[23] J. M. Toledo and V. B. Bezerra, Black holes with a cloud of strings in pure Lovelock gravity, Eur. Phys. J. C **79**, 117 (2019).
[24] M. M. Dias e Costa, J. M. Toledo, and V. B. Bezerra, The Letelier spacetime with quintessence: Solution, thermodynamics and Hawking radiation, Int. J. Mod. Phys. D **28**, 1950074 (2019).
[25] J. M. Toledo and V. B. Bezerra, Some remarks on the thermodynamics of charged AdS black holes with cloud of strings and quintessence, Eur. Phys. J. C **79**, 110 (2019).
[26] J. P. Morais Graça, I. P. Lobo, and I. G. Salako, Cloud of strings in $f(R)$ gravity, Chin. Phys. C **42**, 063105 (2018).
[27] F. F. Nascimento, V. B. Bezerra, and J. M. Toledo, Some remarks on Hayward black hole with a cloud of strings, arXiv:2305.11708.
[28] J. M. Toledo and V. B. Bezerra, Black holes with a fluid of strings, Ann. Phys. (Amsterdam) **423**, 168349 (2020).
[29] J. P. Morais Graça, I. P. Lobo, V. B. Bezerra, and H. Moradpour, Effects of a string cloud on the criticality and efficiency of AdS black holes as heat engines, Eur. Phys. J. C **78**, 823 (2018).
[30] J. M. Toledo and V. B. Bezerra, The Reissner–Nordström black hole surrounded by quintessence and a cloud of strings: Thermodynamics and quasinormal modes, Int. J. Mod. Phys. D **28**, 1950023 (2018).
[31] J. P. Morais Graça, G. I. Salako, and V. B. Bezerra, Quasinormal modes of a black hole with a cloud of strings in Einstein–Gauss–Bonnet gravity, Int. J. Mod. Phys. D **26**, 1750113 (2017).
[32] S. G. Ghosh, U. Papnoi, and S. D. Maharaj, Cloud of strings in third order Lovelock gravity, Phys. Rev. D **90**, 044068 (2014).
[33] G. Panotopoulos and A. Rincón, Minimal geometric deformation in a cloud of strings, Eur. Phys. J. C **78**, 851 (2018).
[34] D. V. Singh, S. G. Ghosh, and S. D. Maharaj, Clouds of strings in 4*D* Einstein–Gauss–Bonnet black holes, Phys. Dark Universe **30**, 100730 (2020).
[35] J. de M. Toledo and V. B. Bezerra, Black holes with cloud of strings and quintessence in Lovelock gravity, Eur. Phys. J. C **78**, 534 (2018).
[36] LIGO Scientific and Virgo Collaborations, Observation of gravitational waves from a binary black hole merger, Phys. Rev. Lett. **116**, 061102 (2016).
[37] LIGO Scientific and Virgo Collaborations, Astrophysical implications of the binary black-hole merger GW150914, Astrophys. J. Lett. **818**, L22 (2016).
[38] LIGO Scientific and VIRGO Collaborations, GW170104: Observation of a 50-solar-mass binary black hole coalescence at redshift 0.2, Phys. Rev. Lett. **118**, 221101 (2017).
[39] LIGO Scientific and Virgo Collaborations, Binary black hole mergers in the first Advanced LIGO observing run, Phys. Rev. X **6**, 041015 (2016).
[40] Event Horizon Telescope Collaboration, First M87 event horizon telescope results. I. The shadow of the supermassive black hole, Astrophys. J. Lett. **875**, L1 (2019).
[41] Event Horizon Telescope Collaboration, First Sagittarius A* event horizon telescope results. II. EHT and multiwavelength observations, data processing, and calibration, Astrophys. J. Lett. **930**, L13 (2022).
[42] M. Okyay and A. Övgün, Nonlinear electrodynamics effects on the black hole shadow, deflection angle, quasinormal modes and greybody factors, J. Cosmol. Astropart. Phys. 01 (2022) 009.
[43] N. Tsukamoto, Z. Li, and C. Bambi, Constraining the spin and the deformation parameters from the black hole shadow, J. Cosmol. Astropart. Phys. 06 (2014) 043.
[44] N. Tsukamoto, Black hole shadow in an asymptotically-flat, stationary, and axisymmetric spacetime: The Kerr-Newman and rotating regular black holes, Phys. Rev. D **97**, 064021 (2018).
[45] R. Shaikh, Black hole shadow in a general rotating spacetime obtained through Newman-Janis algorithm, Phys. Rev. D **100**, 024028 (2019).
[46] R. Shaikh, Shadows of rotating wormholes, Phys. Rev. D **98**, 024044 (2018).
[47] S. Kasuya and M. Kobayashi, Throat effects on shadows of Kerr-like wormholes, Phys. Rev. D **103**, 104050 (2021).
[48] X.-M. Kuang and A. Övgün, Strong gravitational lensing and shadow constraint from M87* of slowly rotating Kerr-like black hole, Ann. Phys. (Amsterdam) **447**, 169147 (2022).
[49] A. Övgün, I. Sakallı, and J. Saavedra, Shadow cast and deflection angle of Kerr-Newman-Kasuya spacetime, J. Cosmol. Astropart. Phys. 10 (2018) 041.
[50] M. Fathi, M. Olivares, and J. R. Villanueva, Spherical photon orbits around a rotating black hole with quintessence and cloud of strings, Eur. Phys. J. Plus **138**, 7 (2023).
[51] S. Vagnozzi, R. Roy, Y.-D. Tsai, L. Visinelli, M. Afrin, A. Allahyari *et al.*, Horizon-scale tests of gravity theories and fundamental physics from the event horizon telescope image of sagittarius a, Classical Quantum Gravity **40**, 165007 (2023).
[52] C. Bambi, K. Freese, S. Vagnozzi, and L. Visinelli, Testing the rotational nature of the supermassive object M87* from the circularity and size of its first image, Phys. Rev. D **100**, 044057 (2019).
[53] A. Belhaj, H. Belmahi, M. Benali, W. El Hadri, H. El Moumni, and E. Torrente-Lujan, Shadows of 5D black holes from string theory, Phys. Lett. B **812**, 136025 (2021).

[54] A. Belhaj, M. Benali, A. E. Balali, W. E. Hadri, and H. El Moumni, Cosmological constant effect on charged and rotating black hole shadows, Int. J. Geom. Methods Mod. Phys. **18**, 2150188 (2021).
[55] S. U. Islam, J. Kumar, R. Kumar Walia, and S. G. Ghosh, Investigating loop quantum gravity with event horizon telescope observations of the effects of rotating black holes, Astrophys. J. **943**, 22 (2023).
[56] R. Kumar Walia, S. G. Ghosh, and S. D. Maharaj, Testing rotating regular metrics with EHT results of Sgr A*, Astrophys. J. **939**, 77 (2022).
[57] R. A. Konoplya and A. Zhidenko, Shadows of parametrized axially symmetric black holes allowing for separation of variables, Phys. Rev. D **103**, 104033 (2021).
[58] A. F. Zakharov, F. De Paolis, G. Ingrosso, and A. A. Nucita, Shadows as a tool to evaluate black hole parameters and a dimension of spacetime, New Astron. Rev. **56**, 64 (2012).
[59] M. Khodadi, G. Lambiase, and D. F. Mota, No-hair theorem in the wake of event horizon telescope, J. Cosmol. Astropart. Phys. 09 (2021) 028.
[60] M. Khodadi and G. Lambiase, Probing Lorentz symmetry violation using the first image of Sagittarius A*: Constraints on Standard Model extension coefficients, Phys. Rev. D **106**, 104050 (2022).
[61] C. Bambi and L. Modesto, Rotating regular black holes, Phys. Lett. B **721**, 329 (2013).
[62] Z. Xu, J. Wang, and M. Tang, Deformed black hole immersed in dark matter spike, J. Cosmol. Astropart. Phys. 09 (2021) 007.
[63] M. Tang and Z. Xu, The no-hair theorem and black hole shadows, J. High Energy Phys. 12 (2022) 125.
[64] B. Carter, Global structure of the Kerr family of gravitational fields, Phys. Rev. **174**, 1559 (1968).
[65] K. Hioki and K.-i. Maeda, Measurement of the Kerr spin parameter by observation of a compact object's shadow, Phys. Rev. D **80**, 024042 (2009).
[66] S. Haroon, M. Jamil, K. Jusufi, K. Lin, and R. B. Mann, Shadow and deflection angle of rotating black holes in perfect fluid dark matter with a cosmological constant, Phys. Rev. D **99**, 044015 (2019).
[67] K. Jusufi, M. Jamil, P. Salucci, T. Zhu, and S. Haroon, Black hole surrounded by a dark matter halo in the M87 Galactic center and its identification with shadow images, Phys. Rev. D **100**, 044012 (2019).
[68] Y. Yang, D. Liu, Z. Xu, and Z.-W. Long, Ringing and echoes from black bounces surrounded by the string cloud, Eur. Phys. J. C **83**, 217 (2023).